LANGMUIR

Article

pubs.acs.org/Langmuir

Site-Specific Modulation of Charge Controls the Structure and Stimulus Responsiveness of Intrinsically Disordered Peptide Brushes

Maniraj Bhagawati,[†] Matt G. Rubashkin,[‡,∥] Jessica P. Lee,[†,§] Badriprasad Ananthanarayanan,[†] Valerie M. Weaver,[‡,∥] and Sanjay Kumar*[,†,∥,▽]

[†]Department of Bioengineering, University of California, Berkeley, Berkeley, California 94720, United States

[‡]Center for Bioengineering and Tissue Regeneration, University of California, San Francisco, San Francisco, California 94143, United States

[∥]UC Berkeley-UCSF Graduate Program in Bioengineering, University of California, Berkeley, Berkeley, California 94720, United States

[§]Department of Chemistry, University of California, Berkeley, Berkeley, California 94720, United States

[▽]Department of Chemical and Biomolecular Engineering, University of California, Berkeley, Berkeley, California 94720, United States

Supporting Information

ABSTRACT: Intrinsically disordered proteins (IDPs) are an important and emerging class of materials for tailoring biointerfaces. While the importance of chain charge and resultant electrostatic interactions in controlling conformational properties of IDPs is beginning to be explored through *in silico* approaches, there is a dearth of experimental studies motivated toward a systematic study of these effects. In an effort to explore this relationship, we measured the conformations of two peptides derived from the intrinsically disordered neurofilament (NF) side arm domain: one depicting the wild-type sequence with four lysine−serine−proline repeats (KSP peptide) and another in which the serine residues were replaced with aspartates (KDP peptide), a strategy sometimes used to mimic phosphorylation. Using a variety of biophysical measurements including a novel application of scanning angle interference microscopy, we demonstrate that the KDP peptide assumes comparatively more expanded conformations in solution and forms significantly thicker brushes when immobilized on planar surfaces at high densities. In both settings, the peptides respond to changes in ambient ionic strength, with each peptide showing distinct stimulus-responsive characteristics. While the KDP peptide undergoes compaction with increasing ionic strength as would be expected for a polyampholyte, the KSP peptide shows biphasic behavior, with an initial compaction followed by an expanded state at a higher ionic strength. Together these results support the notion that modulation of charge on IDPs can regulate conformational and interfacial properties.

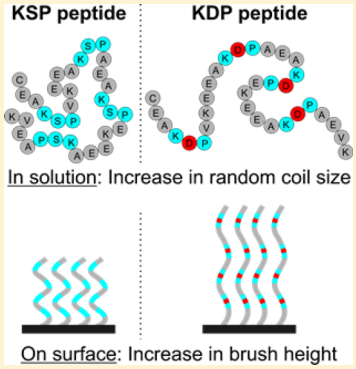

INTRODUCTION

Surface-anchored brushes based on synthetic polymers have been extensively utilized for reducing nonspecific adsorption of materials at solid−liquid interfaces.[1,2] Brushes fabricated from polyelectrolytes and polyampholytes offer the additional possibility of expanding and collapsing in response to changes in their electrostatic milieu.[3−5] Such stimuli-responsive brushes have found numerous applications, including biosensors,[6] separation technologies,[7] and as valves for nanopores.[8] Two important and historically persistent limitations of synthetic polymers are the challenge of precisely controlling chain length and monomeric sequence, both of which strongly influence electrostatic properties. Most polyelectrolytes so far synthesized have therefore either been homopolymers consisting of a single type of charged group,[9,10] random copolymers formed of a combination of two or more chemical species (at least one of which is charged) randomly distributed over the polymer length,[10,11] or block copolymers composed of repeats of discrete charged blocks.[12,13] Constructing polymer brushes from intrinsically disordered proteins (IDPs) offers an opportunity to overcome both of these challenges. Recombinant DNA technology enables the expression and purification of perfectly monodisperse biopolymers with precise placement of charged residues within the protein sequence. The amino acid sequence of IDPs may be tailored to control conformational properties, akin to synthetic polymers.[14] IDPs could also complement synthetic polymers currently used in biomedical applications, e.g., as drug delivery agents,[15−18] cell culture matrices,[19,20] and coatings.[21−23] In principle, non-natural amino acids could be used to introduce additional functionalities, including chemical reactivity and fluorescence.[24] Thus, IDPs are drawing increased interest as biomolecules with unique material properties that can be integrated into biological systems. For example, we recently engineered, expressed, and purified a

Received: March 21, 2016
Revised: May 18, 2016
Published: May 20, 2016

DOI: 10.1021/acs.langmuir.6b01099
Langmuir 2016, 32, 5990−5996

recombinant IDP and showed that this biomolecule could form monodisperse, oriented brushes on surfaces.[25] Furthermore, we showed that these brushes collapse and swell in response to changes in solution ionic strength and pH and that they may be enzymatically shaved to defined heights through the application of proteases directed to specific sequences within the chain. Taken together with analogous studies from other laboratories,[26,27] these findings collectively support broader exploration of IDPs as biomaterials that may be used to tailor interfacial properties in an environmentally responsive fashion.

IDP conformational properties and the resulting interfacial behavior are significantly influenced by electrostatic interactions between charged residues. Recent molecular simulations have revealed the importance of charge position, distribution, and resultant local conformational preferences within an IDP to global IDP structure.[28,29] Despite these important computational advances, there is a need for experimental data connecting IDP charge to interfacial properties. This is particularly important given that many post-translational modifications that may alter the bioactivity of IDPs—most notably phosphorylation—involve additional changes in electrostatic properties not encoded in the original amino acid sequence. Thus, it would be valuable to develop an understanding of how local changes in IDP charge regulate IDP conformation in solution and in the context of a grafted brush.

As a first step toward addressing this question, we have characterized synthetic peptides derived from IDPs with precisely defined differences in chain charge. We based our peptides on the C-terminal projection domain of the human neurofilament heavy subunit (NF-H), which also inspired the full-length recombinant IDPs in our earlier study.[25] This IDP domain extends laterally from the NF core and is thought to sterically stabilize the NF network, which has in turn been hypothesized to contribute to NF network mechanics and axonal caliber.[30−32] Importantly, the human NF-H side arm contains approximately 40−50 lysine−serine−proline (KSP) repeats, which are subject to phosphorylation *in vivo*. The phosphorylation state of these domains has been widely correlated with NF−NF spacing distances. It has therefore been hypothesized that changes in side arm charge can modulate electrostatic repulsion within and possibly between NF side arms, thereby expanding the effective volume occupied by each side arm and increasing NF−NF spacing.[33]

EXPERIMENTAL SECTION

Materials. Fluorescein-labeled as well as unlabeled poly(ethylene glycol) derivatives were purchased from Nanocs, 5-((2-(and-3)-*S*-(acetylmercapto)succinoyl)amino)fluorescein (SAMSA fluorescein) from Thermo Fisher Scientific, and tri(ethylene glycol)undecanethiol from Dojindo Molecular Technologies. All other chemicals were purchased from Sigma-Aldrich. Quartz chips for quartz crystal microbalance were purchased from Biolin Scientific, and gold substrates for surface plasmon resonance were purchased from XanTec Bioanalytics.

Small-Angle X-ray Scattering (SAXS). SAXS measurements were conducted using the SIBYLS beamline at the Advanced Light Source facility of the Lawrence Berkeley National Laboratory. Peptides at a concentration of 1 mg/mL in HEPES buffers of different ionic strengths were analyzed over a scattering vector (q) range of 0.03−0.3/Å with an exposure time of 1 s in triplicate. Similar measurements were also carried out for the different buffer preparations (blank measurements), and the resultant spectra were subtracted from the experimental peptide spectra to obtain the final data. Guinier plots were used to verify that the peptides did not aggregate. The SAXS spectra were then subjected to ensemble-optimized modeling using the ATSAS software package.[34] This analysis is based on the generation of a large pool of theoretical structures (typically 10 000) based on side-chain interaction constraints from the primary sequence of the peptides. The theoretical X-ray scattering profiles calculated from these structures are then matched for fit with the experimental scattering profile to create an ensemble of best-fit structures.

Surface Plasmon Resonance (SPR) Measurements. All SPR measurements were performed at 25 °C in a four flow cell Biacore 3000 instrument (GE Healthcare) on bare gold SPR transducers. KDP peptide and KSP peptides were immobilized on flow channels 1 and 2, respectively, via their N-terminal cysteine residues. Tri(ethylene glycol)undecanethiol, which forms a reference layer, was immobilized on flow channel 3. Immobilization was carried out by injecting 1 mM of the appropriate molecule in HEPES buffer (HBS, pH 7.5, ionic strength 150 mM) into the channels for 40 min at a flow rate of 5 μL/min. All flow channels were subsequently rinsed with the buffer for 30 min to remove any nonspecifically adsorbed material. Following this, injections of BSA in HEPES buffers of various ionic strengths and pH were carried out to measure the heights of the surface layers. Prior to the BSA injections, all flow channels were equilibrated with the appropriate buffer for 15 min. Three injections of BSA (each lasting 1 min, followed by a rinse for 1 min) at a concentration of 1 mg/mL in the corresponding buffer was carried out into all flow channels at a rate of 10 μL/min, with each injection passing all flow channels sequentially. Average response units for each BSA injection was measured relative to the buffer baseline.

Analysis of SPR Data. Immobilization densities (ρ) of the peptides was calculated from the change in the resonance units (ΔRU) by using the relationship 1300 RU = 1 ng/mm^2. The grafting distance (g) could then be calculated from the density using the relationship

$$g\ (\mathrm{nm}) = \sqrt{\frac{M_w \cdot 10^{21}}{N_A \rho}}$$

where M_w is the molecular weight of peptide and N_A is Avogadro's number.

Heights of the layers were calculated from the response of the BSA injections by using the relation

$$H_B = \frac{l_d}{2} \ln\left(\frac{R_{RL}}{R_B}\right) + H_{RL}$$

where H_B and H_{RL} are the heights of the peptide brush and the reference layer (2 nm), respectively, R_B and R_{RL} are the SPR signals during the injection of BSA on the brush and reference layer, respectively, and l_d is the decay length of the surface plasmon. Calculation of optimal l_d for each layer under the various buffer conditions was carried out using the iterative procedure described previously.[35] Modeling of the SPR reflectivity spectrum necessary for the evaluation was done via Fresnel equations using a transfer matrix formalism.[36]

Quartz Crystal Microbalance with Dissipation. QCM-D measurements were performed with a Q-Sense E4 system (Biolin Scientific). Quartz crystals with fundamental frequencies of ∼5 MHz were functionalized with maleimide moieties as described in the Supporting Information and used for immobilization of the peptides. 1 mM of the peptides in HBS was injected into the flow cell at a flow rate of 100 μL/min for 2 min, using a syringe pump. Change in frequency (Δf) and dissipation (ΔD) were measured at five overtones (n = 3, 5, ..., 11) simultaneously. The data were fit using the Voight−Voinova model[37] for viscoelastic films to obtain the surface density of the hydrated peptide layer bound to the surface.

Scanning Angle Interference Microscopy (SAIM) Imaging. The n-type [100]-orientation silicon wafers with 1933 nm silicon oxide (Addison Engineering) were cut into ∼0.5 cm^2 chips using a diamond pen. The substrates were functionalized with the peptides, PEG, and fluorescein as described in the Supporting Information. SAIM calibration wafers were prepared by sonicating carboxylate-modified red fluorescent spheres (100 nm; Invitrogen), following by bead deposition (5 × 10^8 beads per mL) in PBS. Imaging was performed on

DOI: 10.1021/acs.langmuir.6b01099
Langmuir 2016, 32, 5990−5996

an inverted Ti-E Perfect Focus System (Nikon) controlled by Metamorph software, equipped with 488, 561, and 640 nm lasers, a motorized laser Ti-TIRF-E unit, a 1.49 NA 100× TIRF objective, an electron-multiplying charged-coupled device (emCCD) camera (QuantEM 512; Photometrics), and with a linear glass polarizing filter (Edmunds Optics) in the excitation laser path. Imaging and analysis was performed as described previously.[38]

RESULTS AND DISCUSSION

We used solid-phase peptide synthesis to generate two 32-residue peptides based on the NF-H side arm domain. The first peptide contained four KSP motifs (KSP peptide), while in the second the serine residues were replaced with aspartate residues (KDP peptide) (Figure 1A). Comparison of the KSP and KDP peptides is expected to yield insight into electrostatic effects associated with changes in chain charge on IDP structure and stimulus responsiveness. Additionally, as aspartate residues are sometimes used to mimic effects of phosphorylation in proteins, this approach may also lend insight into how serine phosphorylation in these side arm domains contributes to NF structure and interactions in the cytoskeleton.

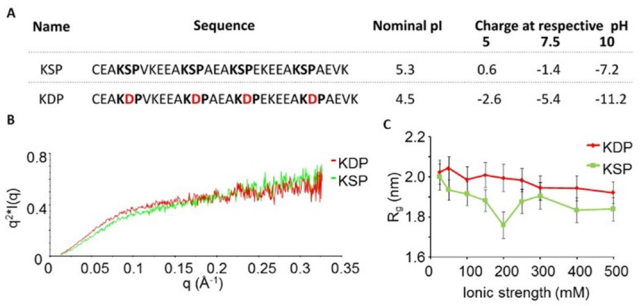

Figure 1. (A) Details of the peptides used in this study. (B) Kratky plots derived from small-angle X-ray scattering (SAXS) of the two peptides dissolved in buffer of ionic strength 150 mM, pH 7.5. (C) Radii of gyration (R_g) of the peptides calculated using ensemble optimized modeling of the SAXS spectra of the peptides in buffers of varying ionic strength at pH 7.5. The error bars represent standard deviations of radii of gyration obtained from EOM modeling of data sets from three SAXS measurements at each ionic strength.

Conformational Dynamics of Peptides in Solution. We first characterized the conformational properties of each peptide in solution using small-angle X-ray scattering (SAXS), which has been extensively applied to capture solution dimensions of both structured and disordered proteins and peptides.[39−41] Kratky plots of the SAXS data for the two peptides in HEPES buffered saline (HBS, ionic strength 150 mM, pH 7.5) reveal a plateau at high value of the scattering vector, q, which is the signature characteristic of random coils (Figure 1B).[39] This confirms that these peptides lack structure, as expected. In order to extract quantitative information on peptide dimensions from the scattering data, we utilized the ensemble-optimized modeling (EOM) method, which has been previously established to be a more potent scheme than the traditional Guinier approach for interpreting SAXS spectra of intrinsically disordered proteins.[34,42] Modeling the data in this fashion, we obtained radii of gyration (R_g) of 2.01 ± 0.06 and 1.88 ± 0.05 nm for the KDP and KSP peptides, respectively.

The lower R_g of the KSP peptide is consistent with recent molecular dynamics (MD) simulations of the C-terminal tails of the NF-H protein,[43] which found that the non-phosphorylated side arm domain is stabilized by salt bridges between glutamate and lysine residues; these attractive electrostatic interactions would presumably be destabilized by the electrostatic repulsions associated with added negative charge upon

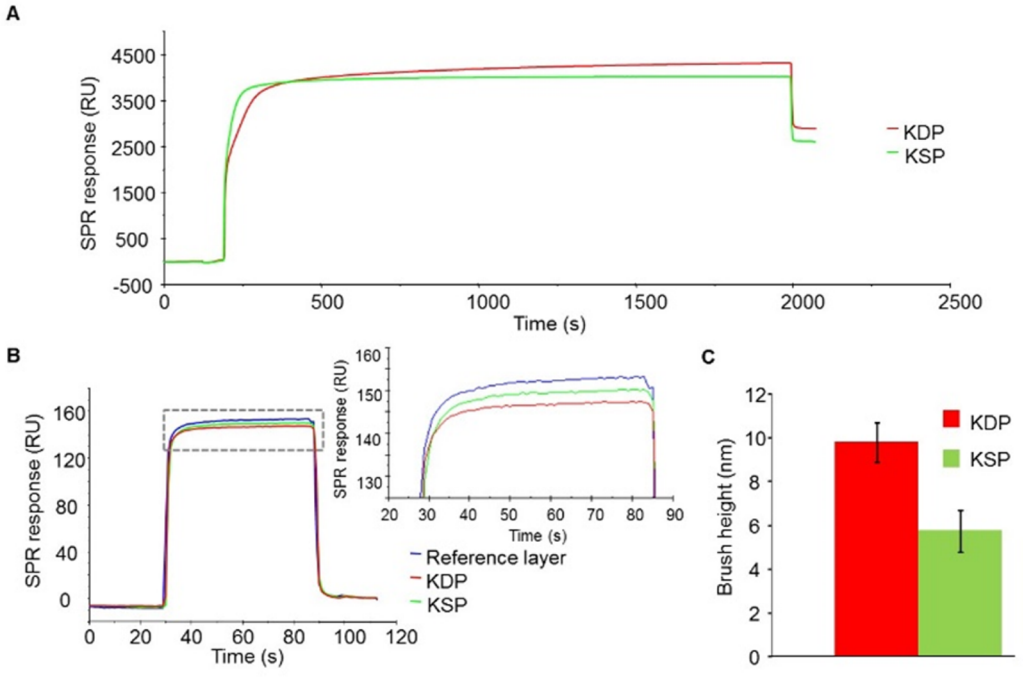

Figure 2. (A) Representative SPR responses for the immobilization of KSP and KDP peptides on SPR transducer surfaces. (B) Representative SPR responses during the injection of BSA dissolved at a concentration of 1 mg/mL in HBS (pH 7.5, ionic strength 150 mM) on surfaces functionalized with KSP and KDP brushes as well as on a reference layer composed of tri(ethylene glycol)undecanethiol. The inset shows an enlarged view of the indicated region. (C) Average heights of KSP and KDP brushes at pH 7.5 and ionic strength 150 mM obtained from three separate experiments. The error bars represent standard errors calculated from the three experiments. Each experiment included three injections of BSA.

DOI: 10.1021/acs.langmuir.6b01099
Langmuir 2016, 32, 5990−5996

phosphorylation. To investigate these electrostatic effects in a more detailed manner, we next conducted SAXS experiments on the peptides as a function of ionic strength. Interestingly, the dependence of R_g on ionic strength for the KSP and KDP peptides (also calculated using EOM, Figure 1C) exhibit distinct behavior. The R_g of KDP decreases monotonically with ionic strength (correlation coefficient $R = -0.94$ between R_g and ionic strength). This is consistent with classical polyelectrolyte theory, which would predict that salt-mediated screening of electrostatic repulsions within the peptide should induce chain condensation. The R_g of the KSP peptide, in contrast, initially falls with increasing ionic strength for ionic strength <200 mM and then rises again for ionic strength >200 mM (correlation coefficient $R = -0.6$ between R_g and ionic strength). Aspects of these trends are predicted by the polyampholyte theory of Higgs and Joanny,[44] which has been previously used for modeling the R_g of short intrinsically disordered proteins of approximately 50 residues in solutions of guanidium hydrochloride.[45] According to this theory, for polyampholytes with high net charge, the R_g is expected to fall with increasing ionic strength, while for polyampholytes with medium net charge, the R_g is expected to fall up to a critical ionic strength, followed by an increase. These trends are qualitatively in tune with our observations, with the nominal net charge on KSP and KDP being −1 (medium) and −5 (high) (7 positive charges for both, and 8 and 12 negative charges for KSP and KDP, respectively). Interestingly, MD simulations of the full-length side arm domain of NF-H show that the R_g of the phosphorylated side arm is expected to decrease with increasing ionic strength as we have observed. For the non-phosphorylated side arm domain, the R_g is expected to remain constant up to an ionic strength of approximately 40 mM, followed by a small increase.[46]

Conformational Dynamics of Peptide Brushes. Having verified the stimulus-responsive properties of these peptides in solution, we next attempted to study their behavior in the form of surface-anchored brushes. This geometry is broadly reminiscent of the *in vivo* arrangement of NF-H side arm domains within the axon, which project from the NF core to form cylindrical brushes. Moreover, as discussed earlier, the potential technological application of surface-grafted IDPs as biologically encoded interfacial materials makes this a very useful paradigm to study.[25−27] We therefore immobilized KSP and KDP peptides via their N-terminal cysteine residues on gold substrates and followed the grafting kinetics using surface plasmon resonance (SPR) (Figure 2A). We calculated grafting densities of 0.46 and 0.5 molecules/nm^2 for KSP and KDP peptides, respectively. Assuming square (two-dimensional cubic) packing, this corresponds to a nearest-neighbor grafting distance of 1.47 nm for KSP and 1.41 nm for KDP. These distances are smaller than the end-to-end distances for the two peptides (4.61 nm for KSP and 4.92 nm for KDP), which can be calculated from the R_g values measured from SAXS (Figure 1C). On the basis of this high surface density, we conclude that the peptides form brushes on the surface. To measure the brush height, we used a SPR-based methodology recently introduced by Schoch et al. in which bovine serum albumin (BSA) is used as a probe to measure the thicknesses of surface-grafted synthetic polymer and protein layers.[35,47] In this method BSA molecules experience a steric repulsive force from the polymer/protein brush (proportional to the excluded volume of the polymer layers), which hinders their approach to the SPR transducer. The SPR response of the BSA molecules is inversely proportional to their average distance from the transducer, which enables calculation of the height of the surface-grafted brush. The SPR response of a solution of BSA in HBS (ionic strength 150 mM, pH 7.5) injected on three different surface layers (Figure 2B) is lowest for a KDP peptide brush, higher for a KSP peptide brush, and highest for a reference layer formed by tri(ethylene glycol)undecanethiol. Analyzing these signals using the procedure described in the Experimental Section, we obtained brush heights of 5.7 and 9.8 nm for the KSP and KDP brushes, respectively (Figure 2C).

We next tested the responsiveness of these peptide brushes to changes in pH. To do this, we injected BSA in HBS of ionic strength 150 mM at different pH (pH 5 and 10) and analyzed the BSA signals following the procedure described above. This showed that the brushes underwent significant collapse at pH 5, shrinking to around half of their previous thickness (Figure 3A). This could be explained by the fact that the nominal

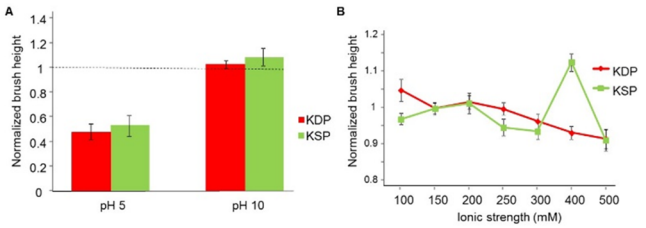

Figure 3. (A) Heights of KSP and KDP brushes at pH 5 and 10 and ionic strength 150 mM normalized to their individual heights at pH 7.5 and ionic strength 150 mM. (B) Heights of KSP and KDP brushes at pH 7.5 and varying ionic strengths normalized to their individual heights at pH 7.5 and ionic strength 150 mM. Three experiments, each consisting of three BSA injections, were conducted, and heights were normalized for each experiment independently. The data presented are the mean and standard error of the normalized heights obtained from the three experiments.

charge on both peptides is lower at pH 5 than at pH 7.5 (Figure 1A). In contrast, both brushes experienced a modest expansion at pH 10, compared to at pH 7.5 (Figure 3A), which again correlates with the increase in the nominal charge on the peptides at pH 10 (Figure 1A). This is consistent with the behavior of a polyelectrolyte or polyampholyte brush, where the brush height depends strongly on chain charge. Furthermore, the extreme sensitivity of the brush height close to the nominal isoelectric point (pI) of the peptide, and comparatively lesser sensitivity at distant pH values is in agreement with our previous measurements with the full-length un-phosphorylated NF-side arm domain.[25] Subsequently, we studied the responsiveness of these brushes to changes in ambient ionic strength at pH 7.5. Again, taking the approach described earlier, we injected BSA in HBS at pH 7.5 of varying ionic strengths and analyzed the SPR signal. We observed significant adsorption of BSA at ionic strengths below 100 mM, possibly due to electrostatic attractive forces between BSA and the brushes, and so we confined our study to ionic strengths >100 mM. In the ionic strength range of 100−500 mM, the brushes demonstrated very interesting and distinct responses to ionic strength (Figure 3B). For the KDP brushes, we observed a continuous decrease in brush height with increasing ionic strength. This behavior agrees with theories developed for polyampholyte and polyelectrolyte brushes, where increasing salt concentration enhances the screening of electrostatic repulsive forces between monomers and thus produces brush

DOI: 10.1021/acs.langmuir.6b01099
Langmuir 2016, 32, 5990−5996

collapse.[48,49] This also correlates with the trend in the R_g of KDP peptide, where increasing ionic strength causes a reduction in the average polymer coil size (Figure 1C). In contrast, the KSP peptide layer is relatively insensitive to ionic strength below 400 mM but undergoes significant expansion at 400 mM, followed by a collapse at 500 mM. While this unexpected behavior is not predicted by relevant mean-field theories, the increase in height of the KSP brush at 400 mM can be hypothesized to be driven by similar mechanisms that cause the high-salt expansion of the KSP peptide at >200 mM in solution (Figure 1C).

A possible criticism of this SPR-based technique for measuring brush height is that it can be affected by adsorption of BSA to the brushes. While we do not observe any significant adsorption of BSA onto peptide-functionalized surfaces in the ionic strengths presented here, we still cannot definitively rule out transient BSA adsorption. To verify these findings with a completely independent methodology, we measured the heights of the peptide brushes using scanning angle interference microscopy (SAIM).[38,50] SAIM measures the optical distance (product of physical distance and the refractive index of the intervening medium) of fluorescent species immobilized on special transducers composed of a thin film of silicon dioxide deposited on a reflective silicon wafer. The intensity of the fluorescence excitation light is axially modulated by varying the angle of incidence. Thus, the fluorescence intensity is a function of the incident angle of excitation light and the distance of the fluorophore from the silicon oxide layer (Figure S1). This angle-dependent variation in intensity is then fit to a model (see Supporting Information for details) to extract the height of the fluorophore above the substrate. While SAIM has been applied with great success to measure intermolecular dimensions within cellular adhesion complexes, it has not as yet been applied to reconstituted polymer brushes. We therefore first verified the ability of SAIM to measure brush heights in a defined system in which thiol-terminated fluorescein-labeled PEG (molecular weight 5000 Da) was covalently immobilized to maleimide-functionalized SAIM substrates at high density. The curve for fluorescence intensity as a function of angle of incidence of excitation light for the PEG brush is shifted to the right of the curve for a comparable substrate that was functionalized with fluorescein (i.e., without the intervening PEG polymer), which confirms the higher thickness of the PEG brush (Figure S2A). On the basis of this observation, we extracted heights of 6 and 15 nm for fluorescein- and PEG-functionalized surfaces, respectively (Figure S2B). The height of the PEG layer could then be calculated as the difference between these two values (9 nm), which agrees with previously published heights of brushes made using PEG of this molecular weight and at comparable density.[35]

Having established SAIM as a suitable method to measure polymer brushes, we attempted to measure the heights of KSP and KDP peptide brushes using this technique. Toward this end, we first synthesized KSP and KDP peptides containing a cysteine on the C-terminus and labeled with fluorescein on the N-terminus. For SAIM studies, we used sequence-reversed retropeptides (PSK rather than KSP repeats; Figure S3A), which facilitated the use of the N-terminus for conjugation of fluorescein on resin, and allowed immobilization via the C-terminal cysteine, while still maintaining the original order of the sequence of amino acids relative to the substrate. We followed the immobilization of these retro-peptides on quartz substrates functionalized with maleimide groups using quartz crystal microbalance with dissipation monitoring (QCM-D) (Figure 4A). We calculated a nearest-neighbor grafting distance

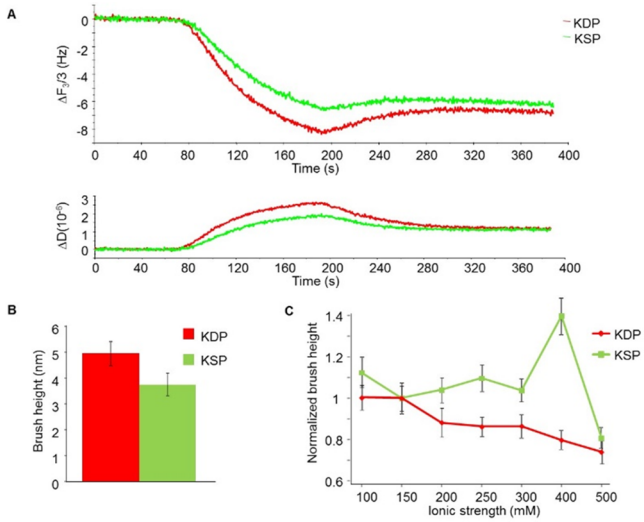

Figure 4. (A) Change in frequency and dissipation (first overtone) signals upon immobilization of KSP and KDP peptides on substrates functionalized with maleimide groups as detected using QCM-D. (B) Heights of KSP and KDP brushes at pH 7.5 and ionic strength 150 mM measured using SAIM. (C) Heights of KSP and KDP brushes measured using SAIM at pH 7.5 and varying ionic strengths normalized to their individual heights at pH 7.5 and ionic strength 150 mM. Three experiments were conducted, and heights were normalized for each experiment independently. The data presented here are the mean and standard error of the (normalized) heights obtained from the three experiments.

of 2.2 nm between each polymer chain using a Voigt−Voinova model to fit the QCM-D data[51] and assuming a square packing of the peptides. While this distance was greater than the grafting distance achieved in the SPR experiments, it was approximately half of the end-to-end distance of the two peptides, ensuring that the immobilized peptides adopted brush conformations. We next measured the heights of the brushes in HBS (ionic strength 150 mM, pH 7.5) using SAIM (Figure 4B). In concurrence with the observations from the SPR-based measurements, we confirmed that the KSP peptide forms a thinner brush than KDP (3.7 and 5.0 nm for KSP and KDP, respectively). The lower heights of the brushes in comparison to the SPR experiments can be explained by the lower surface density in the SAIM experiments. In addition to the different grafting densities, another possible reason for the discrepancy between the heights measured by the two techniques is that the data obtained from the SAIM measurements is modeled using a constant refractive index of the layer (1.33), which may not be strictly correct. In spite of these apparent differences in the absolute brush heights obtained from these two complementary techniques, the strong qualitative agreement between these two independent methodologies supports the notion that KDP peptides form thicker brushes than KSP peptides under comparable grafting densities and solution conditions.

We next conducted SAIM measurements on the peptide brushes under varying ionic strengths. We again observed trends that closely follow the ones observed using the SPR experiments (Figure 4C). KDP peptide brushes displayed a monotonic decrease in brush height with ionic strength. The

DOI: 10.1021/acs.langmuir.6b01099
Langmuir 2016, 32, 5990−5996

brush height of KSP peptides, on the other hand, was largely nonresponsive to ionic strength to 400 mM followed by an abrupt increase at 400 mM and a subsequent drop at 500 mM. Notably, the height of a surface that was functionalized only with fluorescein did not change with ionic strength (data not shown), confirming that the observed brush height variations reflect the dynamics of the peptide brushes rather than any ionic-strength-dependent influences on the underlying surface chemistry or fluorescein fluorescence. As with the comparison between KSP and KDP peptides in solution, these SAIM experiments confirm SPR findings that these two peptides display distinct dependences on ionic strength.

SUMMARY AND CONCLUSIONS

In this report we measured the radii of gyration in solution and heights of surface-grafted brushes formed by two variants of intrinsically disordered peptides that vary by only four amino acids (serine vs aspartate within four KSP repeats). Using SAXS, we established that the KDP peptide assumes more swollen conformations in solution than the KSP peptide. SPR and SAIM measurements reveal that KDP forms thicker brushes than KSP under physiological solution conditions when immobilized on substrates at comparable grafting densities. Notably, our SAIM measurements represent the first use of this methodology to capture heights of immobilized polymer brushes. SAIM has been previously applied to the study of cellular structures using fluorescent protein labels, with height measurements described as accurate to ∼5 nm. In this study we establish that these measurements can be extended to much smaller fluorophores conjugated to purified peptides, which both illustrates the versatility of this interference light microscopy technique and may accordingly yield improvements in measurement accuracy. In conclusion, the measurements presented here are consistent with a hypothesis in which electrostatic effects associated with introduction of very few charged residues in an IDP can strongly modulate conformational and brush properties as well as the dependence of these properties on ionic strength. These results may also have implications for how IDP phosphorylation influences conformational properties and motivates further exploration of phosphorylation (or introduction of phosphomimetic residues) as a useful design tool for engineering material properties of IDPs in solution and at solid−liquid interfaces.

ASSOCIATED CONTENT

Supporting Information

The Supporting Information is available free of charge on the ACS Publications website at DOI: 10.1021/acs.langmuir.6b01099.

Additional details of methods related to peptide synthesis and functionalization of substrates for SPR, QCM-D, and SAIM, supplementary figures describing simulated curves for SAIM, experimental SAIM curves and calculated heights for a fluorescein and a PEG (MW 5000 Da) modified substrate, and sequences of the retro-peptides used in the SIAM measurements (PDF)

AUTHOR INFORMATION

Corresponding Author

*Tel (510) 643-0787; Fax (510) 642-5835; e-mail skumar@berkeley.edu (S.K.).

Notes

The authors declare no competing financial interest.

ACKNOWLEDGMENTS

This work was supported by a PECASE Award from the Army Research Office (W911NF-09-1-0507) to S.K., NIH research program grant (R01CA 192914) to V.M.W., and National Defense Science and Engineering Graduate Fellowship to M.G.R. The authors gratefully acknowledge the support of the Molecular Foundry, Advanced Light Source and the Life Sciences Division of Lawrence Berkeley National Laboratory, with particular thanks to R. Zuckermann and M. S. Tsai. Work at the Molecular Foundry was supported by the Office of Science, Office of Basic Energy Sciences, of the US Department of Energy under Contract DE-AC02-05CH11231. The authors also thank R. Schoch and R. Lim at the Biozentrum, University of Basel, for access to Matlab programs used for analysis of surface plasmon resonance data.

REFERENCES

(1) Welch, M.; Rastogi, A.; Ober, C. Polymer brushes for electrochemical biosensors. *Soft Matter* **2011**, *7* (2), 297−302.
(2) Zauscher, S.; Chilkoti, A. Biological applications of polymer brushes. Preface. *Biointerphases* **2009**, *4* (2), FA1−2.
(3) Das, S.; Banik, M.; Chen, G.; Sinha, S.; Mukherjee, R. Polyelectrolyte brushes: theory, modelling, synthesis and applications. *Soft Matter* **2015**, *11* (44), 8550−83.
(4) Ayres, N.; Cyrus, C. D.; Brittain, W. J. Stimuli-responsive surfaces using polyampholyte polymer brushes prepared via atom transfer radical polymerization. *Langmuir* **2007**, *23* (7), 3744−9.
(5) Pei, Y.; Travas-Sedjic, J.; Williams, D. E. Electrochemical switching of conformation of random polyampholyte brushes grafted onto polypyrrole. *Langmuir* **2012**, *28* (37), 13241−8.
(6) Kurosawa, S.; Aizawa, H.; Talib, Z. A.; Atthoff, B.; Hilborn, J. Synthesis of tethered-polymer brush by atom transfer radical polymerization from a plasma-polymerized-film-coated quartz crystal microbalance and its application for immunosensors. *Biosens. Bioelectron.* **2004**, *20* (6), 1165−76.
(7) Liu, J. X.; Zhao, M. Z.; Deng, Y.; Tie, C.; Chen, H. X.; Zhou, Y. L.; Zhang, X. X. The coating of smart pH-responsive polyelectrolyte brushes in capillary and its application in CE. *Electrophoresis* **2013**, *34* (9−10), 1352−8.
(8) Zeng, Z.; Yeh, L. H.; Zhang, M.; Qian, S. Ion transport and selectivity in biomimetic nanopores with pH-tunable zwitterionic polyelectrolyte brushes. *Nanoscale* **2015**, *7* (40), 17020−9.
(9) Choi, J.; Rubner, M. F. Influence of the Degree of Ionization on Weak Polyelectrolyte Multilayer Assembly. *Macromolecules* **2005**, *38* (1), 116−124.
(10) Barbey, R.; Lavanant, L.; Paripovic, D.; Schüwer, N.; Sugnaux, C.; Tugulu, S.; Klok, H.-A. Polymer Brushes via Surface-Initiated Controlled Radical Polymerization: Synthesis, Characterization, Properties, and Applications. *Chem. Rev.* **2009**, *109* (11), 5437−5527.
(11) Ignatova, M.; Voccia, S.; Gilbert, B.; Markova, N.; Cossement, D.; Gouttebaron, R.; Jérôme, R.; Jérôme, C. Combination of Electrografting and Atom-Transfer Radical Polymerization for Making the Stainless Steel Surface Antibacterial and Protein Antiadhesive. *Langmuir* **2006**, *22* (1), 255−262.
(12) Boyes, S. G.; Akgun, B.; Brittain, W. J.; Foster, M. D. Synthesis, Characterization, and Properties of Polyelectrolyte Block Copolymer Brushes Prepared by Atom Transfer Radical Polymerization and Their Use in the Synthesis of Metal Nanoparticles. *Macromolecules* **2003**, *36* (25), 9539−9548.
(13) Hales, K.; Pochan, D. J. Using polyelectrolyte block copolymers to tune nanostructure assembly. *Curr. Opin. Colloid Interface Sci.* **2006**, *11* (6), 330−336.

DOI: 10.1021/acs.langmuir.6b01099
Langmuir 2016, 32, 5990−5996

(14) Oldfield, C. J.; Dunker, A. K. Intrinsically disordered proteins and intrinsically disordered protein regions. *Annu. Rev. Biochem.* **2014**, *83*, 553−84.
(15) Suk, J. S.; Xu, Q.; Kim, N.; Hanes, J.; Ensign, L. M. PEGylation as a strategy for improving nanoparticle-based drug and gene delivery. *Adv. Drug Delivery Rev.* **2016**, *99* (Pt A), 28−51.
(16) Shroff, K.; Kokkoli, E. PEGylated liposomal doxorubicin targeted to alpha5beta1-expressing MDA-MB-231 breast cancer cells. *Langmuir* **2012**, *28* (10), 4729−36.
(17) Qiu, Y.; Park, K. Environment-sensitive hydrogels for drug delivery. *Adv. Drug Delivery Rev.* **2001**, *53* (3), 321−39.
(18) Banquy, X.; Leclair, G.; Rabanel, J. M.; Argaw, A.; Bouchard, J. F.; Hildgen, P.; Giasson, S. Selectins ligand decorated drug carriers for activated endothelial cell targeting. *Bioconjugate Chem.* **2008**, *19* (10), 2030−9.
(19) Yoshikawa, H. Y.; Rossetti, F. F.; Kaufmann, S.; Kaindl, T.; Madsen, J.; Engel, U.; Lewis, A. L.; Armes, S. P.; Tanaka, M. Quantitative evaluation of mechanosensing of cells on dynamically tunable hydrogels. *J. Am. Chem. Soc.* **2011**, *133* (5), 1367−74.
(20) DeVolder, R.; Kong, H. J. Hydrogels for in vivo-like three-dimensional cellular studies. *Wiley interdisciplinary reviews. Systems biology and medicine* **2012**, *4* (4), 351−65.
(21) Yoshikawa, C.; Qiu, J.; Huang, C. F.; Shimizu, Y.; Suzuki, J.; van den Bosch, E. Non-biofouling property of well-defined concentrated polymer brushes. *Colloids Surf., B* **2015**, *127*, 213−20.
(22) Kusumo, A.; Bombalski, L.; Lin, Q.; Matyjaszewski, K.; Schneider, J. W.; Tilton, R. D. High capacity, charge-selective protein uptake by polyelectrolyte brushes. *Langmuir* **2007**, *23* (8), 4448−54.
(23) Wittemann, A.; Ballauff, M. Interaction of proteins with linear polyelectrolytes and spherical polyelectrolyte brushes in aqueous solution. *Phys. Chem. Chem. Phys.* **2006**, *8* (45), 5269−75.
(24) Wang, L.; Xie, J.; Schultz, P. G. Expanding the genetic code. *Annu. Rev. Biophys. Biomol. Struct.* **2006**, *35*, 225−49.
(25) Srinivasan, N.; Bhagawati, M.; Ananthanarayanan, B.; Kumar, S. Stimuli-sensitive intrinsically disordered protein brushes. *Nat. Commun.* **2014**, *5*, 5145.
(26) Kowalczyk, S. W.; Kapinos, L.; Blosser, T. R.; Magalhães, T.; van Nies, P.; Lim, Y. H. R.; Dekker, C. Single-molecule transport across an individual biomimetic nuclear pore complex. *Nat. Nanotechnol.* **2011**, *6*, 433−438.
(27) Deek, J.; Chung, P. J.; Kayser, J.; Bausch, A. R.; Safinya, C. R. Neurofilament sidearms modulate parallel and crossed-filament orientations inducing nematic to isotropic and re-entrant birefringent hydrogels. *Nat. Commun.* **2013**, *4*, 2224.
(28) Das, R. K.; Pappu, R. V. Conformations of intrinsically disordered proteins are influenced by linear sequence distributions of oppositely charged residues. *Proc. Natl. Acad. Sci. U. S. A.* **2013**, *110* (33), 13392−13397.
(29) Mao, A. H.; Crick, S. L.; Vitalis, A.; Chicoine, C. L.; Pappu, R. V. Net charge per residue modulates conformational ensembles of intrinsically disordered proteins. *Proc. Natl. Acad. Sci. U. S. A.* **2010**, *107* (18), 8183−8.
(30) Brown, H. G.; Hoh, J. H. Entropic Exclusion by Neurofilament Sidearms: A Mechanism for Maintaining Interfilament Spacing. *Biochemistry* **1997**, *36* (49), 15035−15040.
(31) Kumar, S.; Yin, X.; Trapp, B. D.; Hoh, J. H.; Paulaitis, M. E. Relating interactions between neurofilaments to the structure of axonal neurofilament distributions through polymer brush models. *Biophys. J.* **2002**, *82* (5), 2360−2372.
(32) Zhulina, E. B.; Leermakers, F. A. M. The Polymer Brush Model of Neurofilament Projections: Effect of Protein Composition. *Biophys. J.* **2010**, *98* (3), 462−469.
(33) Kumar, S.; Hoh, J. H. Modulation of repulsive forces between neurofilaments by sidearm phosphorylation. *Biochem. Biophys. Res. Commun.* **2004**, *324* (2), 489−96.
(34) Bernado, P.; Mylonas, E.; Petoukhov, M. V.; Blackledge, M.; Svergun, D. I. Structural characterization of flexible proteins using small-angle X-ray scattering. *J. Am. Chem. Soc.* **2007**, *129* (17), 5656−5664.
(35) Schoch, R. L.; Lim, R. Y. H. Non-Interacting Molecules as Innate Structural Probes in Surface Plasmon Resonance. *Langmuir* **2013**, *29* (12), 4068−4076.
(36) Ekgasit, S.; Thammacharoen, C.; Knoll, W. Surface plasmon resonance spectroscopy based on evanescent field treatment. *Anal. Chem.* **2004**, *76* (3), 561−8.
(37) Voinova, M. V.; Rodahl, M.; Jonson, M.; Kasemo, B. Viscoelastic acoustic response of layered polymer films at fluid-solid interfaces: Continuum mechanics approach. *Phys. Scr.* **1999**, *59*, 391−396.
(38) Paszek, M. J.; DuFort, C. C.; Rubashkin, M. G.; Davidson, M. W.; Thorn, K. S.; Liphardt, J. T.; Weaver, V. M. Scanning angle interference microscopy reveals cell dynamics at the nanoscale. *Nat. Methods* **2012**, *9* (8), 825−7.
(39) Receveur-Brechot, V.; Durand, D. How random are intrinsically disordered proteins? A small angle scattering perspective. *Curr. Protein Pept. Sci.* **2012**, *13* (1), 55−75.
(40) Petoukhov, M. V.; Svergun, D. I. Applications of small-angle X-ray scattering to biomacromolecular solutions. *Int. J. Biochem. Cell Biol.* **2013**, *45* (2), 429−37.
(41) Mertens, H. D.; Svergun, D. I. Structural characterization of proteins and complexes using small-angle X-ray solution scattering. *J. Struct. Biol.* **2010**, *172* (1), 128−41.
(42) Bernado, P.; Svergun, D. I. Structural analysis of intrinsically disordered proteins by small-angle X-ray scattering. *Mol. BioSyst.* **2012**, *8* (1), 151−167.
(43) Adiga, S. P.; Brenner, D. W. Molecular Basis for Neurofilament Heavy Chain Side Arm Structure Modulation by Phosphorylation. *J. Phys. Chem. C* **2010**, *114* (12), 5410−5416.
(44) Higgs, P. G.; Joanny, J. F. Theory of polyampholyte solutions. *J. Chem. Phys.* **1991**, *94* (2), 1543−1554.
(45) Müller-Späth, S.; Soranno, A.; Hirschfeld, V.; Hofmann, H.; Rüegger, S.; Reymond, L.; Nettels, D.; Schuler, B. Charge interactions can dominate the dimensions of intrinsically disordered proteins. *Proc. Natl. Acad. Sci. U. S. A.* **2010**, *107* (33), 14609−14614.
(46) Lee, J.; Kim, S.; Chang, R.; Jayanthi, L.; Gebremichael, Y. Effects of molecular model, ionic strength, divalent ions, and hydrophobic interaction on human neurofilament conformation. *J. Chem. Phys.* **2013**, *138* (1), 015103.
(47) Schoch, R. L.; Kapinos, L. E.; Lim, R. Y. Nuclear transport receptor binding avidity triggers a self-healing collapse transition in FG-nucleoporin molecular brushes. *Proc. Natl. Acad. Sci. U. S. A.* **2012**, *109* (42), 16911−6.
(48) Zhulina, E. B.; Birshtein, T. M.; Borisov, O. V. Theory of Ionizable Polymer Brushes. *Macromolecules* **1995**, *28* (5), 1491−1499.
(49) Israels, R.; Leermakers, F. A. M.; Fleer, G. J. On the Theory of Grafted Weak Polyacids. *Macromolecules* **1994**, *27* (11), 3087−3093.
(50) DuFort, C.; Paszek, M. Nanoscale cellular imaging with scanning angle interference microscopy. *Methods Cell Biol.* **2014**, *123*, 235−52.
(51) Voinova, M. V.; Rodahl, M.; Jonson, M.; Kasemo, B. Viscoelastic Acoustic Response of Layered Polymer Films at Fluid-Solid Interfaces: Continuum Mechanics Approach. *Phys. Scr.* **1999**, *59* (5), 391.

DOI: 10.1021/acs.langmuir.6b01099
Langmuir 2016, 32, 5990−5996